Journal of Membrane Science 523 (2017) 36–44

Contents lists available at ScienceDirect

Journal of Membrane Science

journal homepage: www.elsevier.com/locate/memsci

Impact of ion exchange membrane surface charge and hydrophobicity on electroconvection at underlimiting and overlimiting currents

K.A. Nebavskaya[a], V.V. Sarapulova[a], K.G. Sabbatovskiy[b], V.D. Sobolev[b], N.D. Pismenskaya[a], P. Sistat[c], M. Cretin[c], V.V. Nikonenko[a,*,1]

[a] Kuban State University, Stavropolskaya st., 149, Krasnodar, Russia
[b] Frumkin Institute of Physical Chemistry and Electrochemistry RAS, Leninsky prospect 31, Moscow, Russia
[c] European Membrane Institute, University of Montpellier, Place Eugèfigne Bataillon, Montpellier Cédex 5, France

ARTICLE INFO

Keywords:
Ion exchange membrane
Surface charge
Surface hydrophobicity
Electroconvection
Zeta-potential

ABSTRACT

The mechanism of electroconvection at a permselective surface presents a high interest for electrodialysis separation processes as well as for microfluidics and other applications. We have studied a commercial Neosepta AMX-Sb anion-exchange membrane and its three modifications differing in the surface charge and, as a consequence, in the degree of hydrophobicity. The zeta-potential and the contact angle were measured; the membranes were characterized by chronopotentiometry and voltammetry. It is shown that at the current densities slightly lower or equal to the limiting current density, the mass transfer rate is mainly affected by the membrane surface charge. However, at the higher current densities, the main factor is the degree of hydrophobicity: the samples with a weakly charged highly hydrophobic surface show lower voltage under the same current density. This peculiarity is explained by the fact that the mechanism of electroconvection (EC) depends on the current density. At underlimiting currents and low voltages, EC occurs as electroosmosis of the first kind; the surface charge determines the parameters of the (quasi)equilibrium electric double layer (EDL), playing the main role in the phenomenon. At overlimiting currents and high voltages, it is the extended space charge region (much thicker than the EDL), which controls EC occurring apparently as electroosmosis of the second kind (nonequilibium EC). Then the contribution of the EDL is less important, while the impact of hydrophobicity increases. It is shown that the equilibrium EC may be quite strong at the AMX-Sb membrane having a highly developed surface roughness of different scales. In the range of 0.03–0.06 V there is an "anomaly": with increasing current density the potential drop over the AMX-Sb is decreasing instead of increasing.

1. Introduction

Electrodialysis is widely used for production of potable water from brackish water sources, as well as for production of high quality industrial process water or treatment of certain industrial effluents [1]. Its broader employment is hindered by the low mass transport rate when treating the dilute solutions [2], mainly due to the decrease of electrolyte concentration at ion exchange membrane/solution boundary caused by the passage of electric current [3]. Under condition that electrodiffusion is the only mechanism of mass transfer, the formation of such a concentration gradient (known as concentration polarization) leads to the phenomenon of limiting current (i_{lim}), which is attained when the concentration gradient reaches its maximum value. This state relates to the nearly vanishing electrolyte concentration at the surface. However, the limiting current may be exceeded if additional mass transfer mechanisms, such as gravitational convection or electroconvection [4,5], arise, or new charge carriers are produced by water splitting [6,7] or ampholyte dissociation. In dilute solutions, EC, which is caused by the action of electric force on space charge in the depleted solution near the ion selective surface, is of major importance.

EC aids to mix the solution near the ion exchange surface, which enhances the mass transfer rate in electrodialysis. Along with electrodialysis, this phenomenon is important, and even makes the basis of functioning, for micro- and nanofluidic devices, such as electrokinetic micropumps, nanomixers [8] and other [9]. It is significant in analytical chemistry for solution pre-concentration [10], in the processes of electro-sedimentation [11], electrophoresis and others.

Generally, space charge region (SCR) at ion-exchange membrane

* Corresponding author.
E-mail addresses: littlegreenchemist@yandex.ru (K.A. Nebavskaya), sabbat07@mail.ru (K.G. Sabbatovskiy), marc.cretin@iemm.univ-montp2.fr (M. Cretin).
[1] v_nikonenko@mail.ru

http://dx.doi.org/10.1016/j.memsci.2016.09.038
Received 12 September 2016; Received in revised form 22 September 2016; Accepted 23 September 2016
Available online 24 September 2016

(IEM) surface involves equilibrium electric double layer (EDL), which occurs at the surface even in the absence of electric current, and extended SCR, which forms when the current density exceeds i_{lim} [4]. When a current flows across an ion-exchange membrane, electrolyte interfacial concentration, C_s, decreases (in the depleting solution). The (quasi)equilibrium EDL thickness, λ, increases being proportional to $(C_s)^{-1/2}$, but its structure remains unchanged. The extended SCR is essentially non-equilibrium, it appears when $C_s \ll C_O$ (C_O is the electrolyte concentration in the bulk solution). While λ is of the order of nanometer, the thickness of the extended SCR can be a few μm [12]. Depending on what part of the SCR the electric force is applied, electroconvection may be equilibrium or nonequilibrium [13]. Usually, equilibrium EC is considered as the classical electroosmosis (EO), i.e. a fluid slip along the surface induced by the tangential component of applied electric force. When an electric force is applied to a SCR involving its extended part, two situations are possible. If the electric force contains its tangential component, EC can occur in EO mode (as a slip). Dukhin and Mishchuk [14–16] call this mechanism "EO of the second kind" (keeping term "EO of the first kind" to the classical EO, where no extended SCR appears). EO of the second time may be stable or instable, when a certain voltage threshold is overcome. According to Mishchuk et al., [17], to produce this kind of EC, two sufficiently high components of electric field are needed. The normal one is to form an extended SCR, and a tangential one, to yield the fluid slip.

However, even in the condition where no tangential field is applied, intensive EC is possible due to electro-osmotic instability discovered by Rubinstein and Zaltzman [18]. This kind of electroconvection arises, when a small perturbation of concentration or electric or fluid velocity fields does not decay with time, but induces higher deviations from the steady state. In this case, oscillations of potential (when the current is fixed) or current (when the potential is fixed) are observed in simulations [18–22], as well as in experiments [23–25]. In particular, tangential component of electric field arises changing its magnitude and direction with time.

Since EDL is always present at charged surfaces of ion exchange membranes, equilibrium EC occurs in no threshold mode. At the same time, unstable non-equilibrium electroconvection (both the Rubinstein-Zaltzman or Dukhin-Mishchuk modes) requires some threshold value of potential drop to be reached. At small excesses of overlimiting current density (at potential drops about 0.3 V across one membrane) the extended SCR is formed, but EC can be stable [20]. At further increase of potential drop (to about 1 V), the transition to regime of electrokinetic instability occurs [18,26].

Until recently it was thought [26] that only the non-equilibrium EC can cause oscillations of potential drop under a constant current. Zholkovskij et al. [27] have shown theoretically that equilibrium EO near a perfectly perm-selective surface cannot yield instability. However, in their recent work [13], Rubinstein and Zaltzman have predicted theoretically that the oscillations of current caused by equilibrium EC can arise, if the membrane is not ideally selective. In Refs. [28,29], it was found experimentally that, really, in some cases (undulated membrane surface, alternation of well and poorly conductive regions on the membrane surface, its high hydrophobicity) these oscillations are observed in transition regime at small potential drops and at times significantly lower than the transition time.

The velocity of electroosmotic slip, u, caused by equilibrium EO, is a strong function of the surface charge. According to Rubinstein and Zaltzman [13,26], u increases with zeta potential ζ as:

$$u = \left(\zeta \frac{F}{RT} \left(\frac{F}{RT} \frac{\partial \varphi}{\partial x} + \frac{1}{C} \frac{\partial C}{\partial x} \right) - \frac{4}{C} \frac{\partial C}{\partial x} \ln \frac{1+e^{\left(\frac{\zeta F}{2RT}\right)}}{2} \right) \frac{\varepsilon \varepsilon_0 (RT)^2}{4\pi \eta F^2} \quad (1)$$

where C is the electrolyte concentration, T is the absolute temperature, η is the dynamic viscosity of solution, F =96485 C mol^{-1} is the Faraday constant, R =8.314 J mol^{-1} K^{-1} is the gas constant, ε is the relative permittivity of solution, ε_O =8.85 10^{-12} F·m^{-1} is the vacuum permittivity. ζ is defined as the potential drop between the slip plate and the outer border of EDL, its value increases with surface charge, σ, according to the Grahame equation [30]:

$$\sigma = \sqrt{8\varepsilon\varepsilon_0 CRT} \times \sinh\left(\frac{\zeta F}{2RT}\right) \quad (2)$$

Eq. (1) is a generalization of the Smoluchowski equation deduced when accounting for polarization of the EDL by the applied tangential electric field [13]. The relation between the surface charge and intensity of EC was also theoretically discussed by Andersen et al. [31], who connected the propensity to develop electroosmotic instability with the membrane surface charge density, which can be a function of applied current. When H^+ and OH^- ions are generated at the depleted surface (water splitting), the surface charge can be reduced, e.g. due to deprotonation of fixed amino groups (current-induced discharge [31]).

Generally, it is possible to change the value of surface charge (by changing the concentration of the fixed ions on the surface of IEM or by charging the surface of channels in microfluidic devices [32]). Hence, it is important to study how ion transport and electroconvection respond to the variation of membrane surface charge. However, as far as we know, no such studies were carried out.

As it is follows from Eqs. (1) and (2), with increasing σ (ζ), electroconvection should increase. However, there is another factor, which affects EC. Really, when increasing surface charge, its hydrophobicity will decrease. Nevertheless, as it was shown experimentally [33,34] and via simulation [20,35], increasing hydrophobicity leads to increasing overlimiting transfer caused by a more intensive EC. This effect is explained by easier fluid slip over the highly hydrophobic regions [36]. Properties of water near a hydrophobic surface differ from those of bulk water. There is local reduction of water density [37–39], which is accompanied by a decrease in the viscosity [40] and in dielectric permittivity [37], which in turn compresses the EDL. The change in water properties affects the velocity of electroosmotic slip at a hydrophobic surface [37,41–43].

There is a number of studies where the tangential streaming potential/zeta potential was measured for ultrafiltration and reverse osmosis membranes [44–48]. In particular, Szymczyk et al. [47] found that a chemical modification of an UF membrane leads to a charge reversal (from negative to positive) of the porous substructure of the membrane, while the overall charge of the external surface remains negative, although with diminished magnitude. However, only few of papers reported the results of similar measurements for ion-exchange membranes [49,50]. Lee et al. characterized the AEM fouling in terms of zeta potential [51]. A new promising method for determening the lateral electrical conductivity of ion-exchange membranes based on the measurements of tangential streaming current and streaming potential was developed by Sedkaoui et al. [50].

In this work we prepare a series of ion-exchange membranes with similar properties, but differing in surface charge and, as a consequence, in the degree of hydrophobicity. To evaluate the surface charge, we measure the tangential streaming potential and then determine the zeta potential and use Eq. (2) to find σ. By applying chronopotentiometry and voltammetry, we try to find out how the membrane surface properties affect the development and mechanism of electroconvection at low and high voltages.

2. Experimental

2.1. Membranes

We studied a Neosepta AMX-Sb homogeneous anion exchange membrane (manufactured by Astom, Japan) and three its modifications. The AMX-Sb sample was prepared from a commercial membrane subjected to standard salt pretreatment. Additionally, we stu-

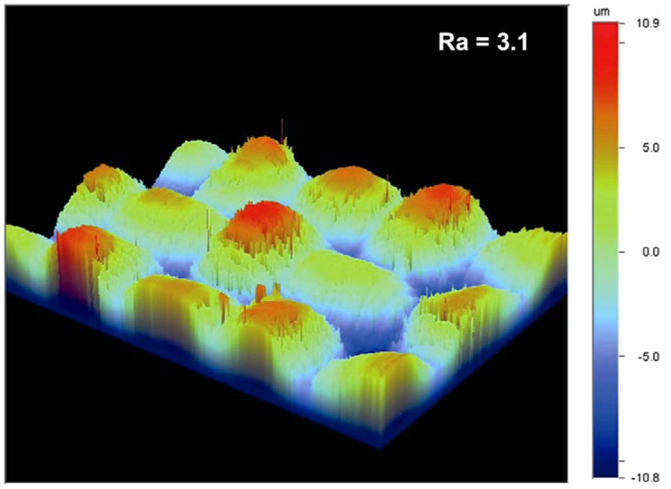

Fig. 1. 3D images of AMX-Sb surface morphology obtained via optical interferometry. Dimensions of the investigated sample were 1257×942 μm×μm. Reproduced with permission from [52].

died: (1) AMX-Sb_{used} produced from the commercial membrane after 30 h of its operation at direct current of 6 mA cm^{-2}; (2) AMX-Sb_{mod1} and (3) AMX-Sb_{mod2} obtained by casting on the surface of AMX-Sb one and two thin layers of MF-4SK from its 1% (weight) dispersion in isopropyl alcohol, respectively. MF-4SK is a perfluorinated membrane carrying sulfonic groups (an analogue of Nafion) manufactured by Plastpolimer, Russia.

Visualization of AMX-Sb surface via optical interferometry realized by Güler et al. [52] shows that reinforcing cloth embedded in the membrane provides an undulated surface. There are "hills" separated by "valleys" (Fig. 1). The distance between two neighboring hills is about 350–400 μm, the difference between the highest and the lowest points is equal to b =22 μm. There is also the undulation of smaller scales, the arithmetic average of the absolute values of the visible roughness profile ordinates is listed as R_a =3.1 μm.

Our optical micrographs (Fig. 2) show that the surface of swollen AMX-Sb membrane possesses the repeating hills with period of about 480 μm and b=20 μm. Optical micrographs of cross section of the modified membranes allow one to evaluate the thickness of the modifying MF-4SK film as 5 μm maximum. However, this film is uneven over the surface, it is concentrated mainly in "valleys" of the membrane, there are areas where it is absent. The second layer (nearly of the same thickness) is distributed more uniformly.

The main physico-chemical and electrochemical properties of AMX-Sb membrane are present in Table 1.

It is known [55–58] that the operation of anion exchange membranes at overlimiting currents leads to partial transformation of its quaternary ammonium groups into secondary and tertiary amines, which are uncharged at neutral pH [59]. Hence it could be expected that the absolute value of charge and zeta potential of AMX-Sb_{used} sample would be lower than those of the commercial membrane.

As the MF-4SK carries sulfonic fixed groups with opposite charge sign in relation to the quaternary ammonium groups of AMX-Sb, we can expect that the surface charge of AMX-Sb_{mod1} and AMX-Sb_{mod2} will be less positive (or even negative) compared to the unmodified membrane. The thickness of each casted layer is estimated as 5 μm,

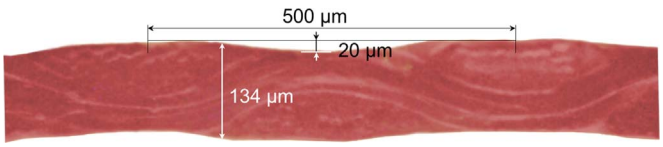

Fig. 2. Optical micrograph of cross section of a swollen AMX-Sb membrane. The threads of reinforcing cloth are visible.

Table 1
Main properties of AMX-Sb membrane.

Manufacturer	Astom, Japan[a]
Type	homogeneous, strong base[a]
Thickness (μm)	140[a]/134[b]
Conductivity in 0.02 M NaCl solution, S m^{-1}	0.32[b]
Ion exchange capacity (meq g^{-1})	1.30 ± 0.05[c]
Water content (g H_2O·(g dry membrane)$^{-1}$)	0.10–0.14[c]
Membrane density (g cm^{-3})	1.10[c]

[a] Manufacturer data [53].
[b] Our measurements.
[c] [54].

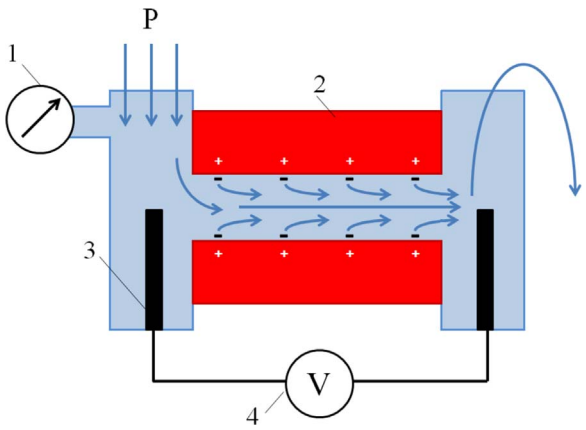

Fig. 3. Scheme of the gap cell for measurement of streaming potential. 1 – pressure gauge, 2 – studied samples, 3 – Ag/AgCl electrode, 4 – multimeter.

while the thickness of AMX-Sb is 134 μm.

2.2. Electrokinetic characteristics

The gap cell used for measuring zeta potential of IEMs is described in Ref. [60] and schematically shown in Fig. 3. It is similar to that applied in the Anton Paar SurPass 3 electrokinetic analyzer. The latter one was employed by Yaroshchuk and Luxbacher [44] for measuring external and internal (inside membrane pores) zeta-potential, as well as by Sedkaoui et al. [50], who developed a promising method for determining the lateral conductivity of ion exchange membranes from the measurements of the streaming current and streaming potential. In our cell, two samples under study form a slit rectangular channel of 25 mm length, 2 mm width, and 70 μm height. The experiments were conducted at 20 °C, using a 0.02 M NaCl solution pumped with a linear velocity of 40–70 cm s^{-1}.

Streaming potential was registered in the range of pressure drops between 0.125 and 0.625 bar with help of two Ag/AgCl electrodes (Fig. 3) using a GW Instek multimeter, connected through a U5-12 amplifier.

2.3. Electrochemical characteristics

Chronopotentiograms and current-voltage characteristics are obtained for commercial and modified membranes using a flow-through four-chamber cell previously described in [28].

To form one desalination chamber, one concentration chamber and two electrode chambers, a membrane under study and two auxiliary membranes, one AMX-Sb and one CMX (Astom, Japan) are used. The all chambers are fed with the same solution, 0.02 M NaCl. The feature of the cell is the special input and output devices, which ensure laminar flow of the solutions between the membranes. The polarized membrane area is S=2×2 cm^2, the intermembrane distance is h=6.5 mm, the average linear flow velocity is V=0.46 cm s^{-1}, the measurements were conducted at 25 °C. The "theoretical" limiting current i_{lim}^{theor} is

calculated using the Leveque equation [61]:

$$i_{lim}^{theor} = \frac{z_1 C_1 FD}{h(T_1 - t_1)}\left[1.47\left(\frac{h^2 V}{LD}\right)^{1/3} - 0.2\right] \quad (3)$$

where C_1 and z_1 are the molar feed concentration and the charge number of the counterion, respectively, D is the electrolyte diffusion coefficient in solution, T_1 and t_1 are counterion transport numbers in membrane and in solution, respectively, L is the length of desalination path. For the experiment conditions, i_{lim}^{theor} according to Eq. (3) is 3.12 mA cm^{-2}, D is taken for the infinitely dilute solution, D=1.61×10^{-9} m^2 s^{-1}. The corresponding value of the diffusion layer thickness δ, found using the Peers equation [28] for i_{lim}=3.12 mA cm^{-2}, is 250 μm.

A potentiostat/galvanostat AutoLab PGSTAT100 is used to apply DC current and to record the current density and the potential drop. The potential drop, Δφ, is measured between two Luggin capillaries whose tips are installed at both sides of the studied membrane against the geometrical center of its polarized area at a distance of about 1 mm from its surface. Current-voltage characteristics are obtained by sweeping the current in the range from 0 to 5.0 mA cm^{-2} (that is from 0 to 1.6 i_{lim}^{theor}) with the rate 2.5×10^{-6} A cm^{-2} s^{-1}.

Experimental chronopotentiograms are obtained in the range of current densities from 1.5 to 7.0 mA cm^{-2} (from 0.48 to 2.24 i_{lim}^{theor}).

2.3.1. Theory of tangential streaming current/potential

To express the zeta potential, ζ, from the measured tangential streaming potential ΔE of membranes, most frequently [48,49,62,63] the classical Helmholtz-Smoluchowski equation is applied:

$$\zeta = \frac{\Delta E}{\Delta P}\frac{\eta \kappa_0}{\varepsilon \varepsilon_0} \quad (4)$$

where κ_O is the conductivity of the solution feeding the gap cell, ΔP is the pressure drop over the channel formed by the membranes.

However, this equation does not take into account the conduction of the walls, i.e. the membrane body in our case. For the first time, this account was made by Yaroshchuk and Ribitsch [64] and then applied by Yaroshchuk and Luxbacher [44], Fievet et al. [45] and Szymczyk et al. [44,50] for determination of zeta-potential and Sedkaoui et al. [50] for finding membrane lateral conductivity.

Let us consider the system, which involves two membranes of length L forming a slit channel of height h and width H filled with a solution. A pressure difference between the two ends of the channel, ΔP, drives the liquid through the channel. Since the fluid near the membrane interfaces carries an excess of charge equal to σ, its motion will produce an electric current known as streaming current, I_s. The local streaming current density is equal to the product of local tangential fluid velocity, $v(x)$, and local electric charge density, $\rho(x)$. The total streaming current is obtained by the integration over the channel cross section:

$$I_s = 2\int_l \left(\int_{sp}^{\frac{h}{2}} \rho(x)v(x)dx\right)dl \quad (5)$$

The line integral is taken along the curve following the membrane surface cross section (Fig. 4). x is the normal to the membrane surface coordinate, it varies from the slip plane (sp) [65] to the half channel (h/2). Below we make the integration ($sp \le x \le h/2$) while assuming that the membranes are identical.

Following Yaroshchuk and Ribitsch [64], we take into account that $\rho(x)$ satisfies the Poisson equation, $\varphi''(x) = -\rho(x)/\varepsilon\varepsilon_0$, where $\varphi(x)$ is the local electrostatic potential. $\varphi(x)$ is subject to the boundary conditions: $\varphi(sp)=\zeta$, $\varphi(h/2)=\varphi'(h/2)=0$. The fluid velocity satisfies the Stokes equation, $\eta v''(x) = \Delta P/L$, for steady laminar flow in a slit channel, with the following boundary conditions: $v(sp)=0$ and $v'(sp) = -(\Delta P/L)(h/2\eta)$.

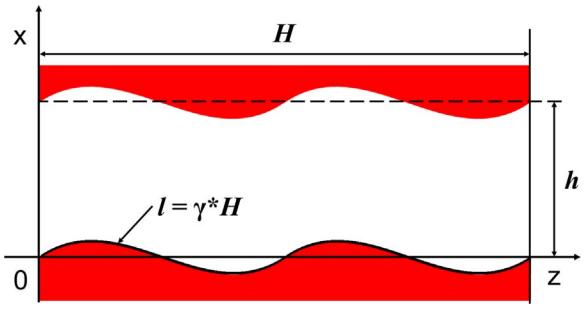

Fig. 4. Scheme of the slit channel cross section in the gap cell for electrokinetic measurements. H is channel width, γ is the ratio between the true length l of the membrane surface cross-section line and its projection on z axis, h is the intermembrane distance. The membrane surface is identified with the slip plane.

The last condition follows from the integration of the Stokes equation from sp to $h/2$ when taking into account the symmetry of the velocity profile imposing $v'(h/2)=0$. In this consideration we assume that the deviation of the line following the slip plane at the surface from the median straight line (Fig. 4) is small compared to $h/2$.

Substituting the Poisson equation into the internal integral in Eq. (5) gives $-\varepsilon\varepsilon_0\int_{sp}^{\frac{h}{2}} v(x)\varphi''(x)dx$. After taking the last integral two times by parts and applying the boundary conditions, we find:

$$\int_{sp}^{\frac{h}{2}} \rho(x)v(x)dx = -\varepsilon\varepsilon_0\int_{sp}^{\frac{h}{2}} v(x)\varphi''(x)dx = \varepsilon\varepsilon_0\frac{h}{2\eta}\frac{\Delta P}{L}\left(\zeta - \frac{2}{h}\int_{sp}^{\frac{h}{2}} \varphi(x)dx\right) \quad (6)$$

Zeta-potential appears in the last expression due to boundary condition $\varphi(sp)=\zeta$. The integral term in the right-hand side of Eq. (5) in relatively wide channels (of the order of several tens of μm) is very small [64], since φ(x) has essentially non-zero values only within the EDL (of the order of several nm); it can be neglected. Substituting Eq. (6) into Eq. (5) yields

$$I_s = \frac{\varepsilon\varepsilon_0 \gamma H h}{\eta}\frac{\Delta P}{L}\zeta \quad (7)$$

where γ is the ratio of the true length of the membrane surface cross-section line to its projection onto the z-axis.

The measurement of the streaming current is only possible if the extremes of the channel are connected through a low-resistance external circuit (short-circuit conditions) [64,65]. If the resistance of the external measuring instrument is high (open circuit, a high-impedance voltmeter used, Fig. 3), transport of ions by the streaming current results in the accumulation of charges at the channel ends. This separation of charges gives rise to a potential difference across the channel length, the streaming-potential, ΔE. ΔE generates conduction current, I_c, which is governed by the Ohm law:

$$I_c = -G\Delta E = -(\kappa_0 H h + 2\kappa_m H d_m)\frac{\Delta E}{L} \quad (8)$$

where G is the system conductance; d_m and κ_m are the thickness and specific conductance (conductivity) of the membrane, respectively. G is calculated for a circuit, consisted of three resistances in parallel: the slit solution channel and two membranes [45,64]. Here for expressing the cross section available for ion transport in solution, we do not take into account the membrane surface undulation, as the hills and the valleys cancel each other regarding solution conductance.

In conditions of measurements of the streaming potential, the net current vanishes. The streaming current, I_s, which always occurs (as breaking circuit does not disturb the normal distribution of concentrations, $c_i(x)$ and the tangential velocity $v(x)$) is compensated by the conduction current [65,66]. Summing Eqs. (7) and (8) with condition $I_s + I_c = 0$ yields:

$$\zeta = \frac{\Delta E}{\Delta P}\frac{\eta\kappa_0}{\varepsilon\varepsilon_0\gamma}\left(1 + 2\frac{\kappa_m d_m}{\kappa_0 h}\right) \quad (9)$$

An equation equivalent to Eq. (9) was first obtained by Yaroshchuk and Ribitsch [64] in the case of a smooth membrane surface, i.e. when γ=1. It was then used by Fievet et al. [45] for evaluation of zeta potential of a ceramic membrane.

Note that when $\frac{\kappa_m d_m}{\kappa_0 h}$ «1, Eq. (9) is reduced to the Helmholtz-Smoluchowski equation, Eq. (4). The sense of parameter $\frac{\kappa_m d_m}{\kappa_0 h}$ is similar to that of the Dukhin number expressing the ratio of the surface conductance to the solution bulk conductance [65]: $Du = \frac{\kappa_\sigma}{\kappa_0 h}$, where κ_σ is the surface conductivity. When the surface conductance is taken into account, the total system conductance will be $G = (\kappa_0 Hh + 2\kappa_m H d_m + 2\kappa_\sigma H)/L$, and Eq. (9) can be generalized:

$$\zeta = \frac{\Delta E}{\Delta P}\frac{\eta\kappa_0}{\varepsilon\varepsilon_0\gamma}\left(1 + 2\frac{\kappa_m d_m}{\kappa_0 h} + 2Du\right) \quad (10)$$

However, as we mentioned above, the surface conductance is negligible in the considered system, as the EDL thickness is 4 orders of magnitude less than h: $Du \ll 1$.

In our system (Fig. 3), an excessive pressure is applied in the left–hand solution, hence, $\Delta P < 0$. The solution flows from the left to the right, $v > 0$, then the streaming current is negative, $I_s < 0$, since it is transferred by the negative charges dominating at the positively charged surface of an anion-exchange membrane. When the circuit is broken, the streaming current leads to accumulation of negative charges at the right, and the positive ones, at the left. This separation of charges generates a positive electric field and a negative streaming potential, $\Delta E < 0$. The conduction current is positive, $I_c > 0$. The zeta-potential near a positively charged surface is positive, $\zeta > 0$.

3. Results and discussion

A typical chronopotentiogram, i.e. potential difference as a function of time, obtained using the procedure described above, and its derivative, d(Δφ)/dt, are shown in Fig. 5. An important characteristic of the chronopotentiograms measured at an overlimiting current is the transition time, τ. It corresponds to the change in ion transport mechanism: from electrodiffusion to a more complex mechanism, where current-induced convection and water splitting make their contribution. This change results in decreasing rate of the interfacial concentration, C_s, decline with time, and, as a consequence, to slowing down Δφ(t) growth. The experimental transition time, τ_{exp}, is determined by the inflection point of chronopotentiogram relating to the maximum of the derivative d(Δφ)/dt.

The transition time may be calculated using the Sand equation [68]

$$\tau_{Sand} = \frac{\pi D}{4}\left(\frac{Fz_1C_1}{T_1 - t_1}\right)^2\frac{1}{i^2} \quad (11)$$

deduced from the Nernst-Planck equation when assuming a stagnant diffusion layer of infinite thickness near the membrane / electrode. Eq. (11) gives generally underestimated values of τ, as ignores convective contribution to the ion transport (due to the forced or natural convection). However, if the current density is sufficiently high, electrolyte interfacial concentration vanishes so rapidly that the developing concentration profile does not attain the distance where the convective ion transport towards the membrane is significant [69]. According to simulations [69,70], the Sand equation may be applied at $i > 2i_{lim}$.

When a finite-length diffusion boundary layer is considered, the contribution of the convective ion transport is implicitly taken into account. We have used the non-stationary three-layer model described in [67] to calculate the "theoretical" chronopotentiograms. In this model, an ideally selective membrane (non-permeable for co-ions) and

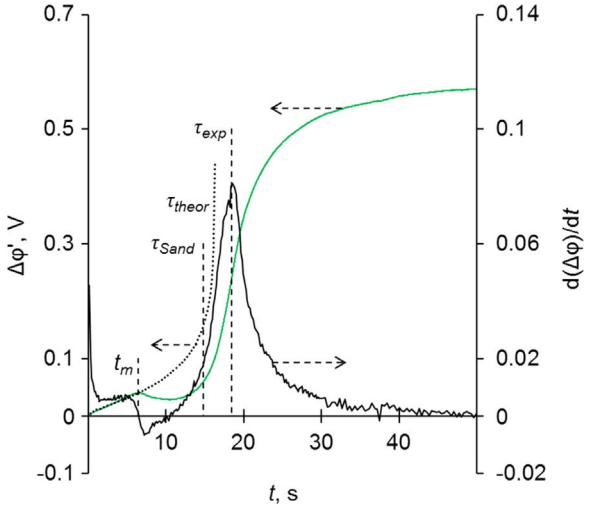

Fig. 5. Chronopotentiogram obtained for an AMX-Sb membrane in a 0.02 M NaCl solution at i=4.5 mA cm^{-2} (i/i_{lim}^{theor}=1.44) and its derivative; the both are shown with solid lines. The chronopotentiogram calculated numerically according to a three-layer model [67] is presented by the dotted line. τ_{exp}, τ_{Sand}, and τ_{theor} relate to three different values of the transition time: the experimental value (found by the inflection point), the value calculated using the Sand equation, and the "theoretical" value (found using model [67]), respectively. t_m shows the time of appearance of the first oscillation of potential drop. Δφ' is the potential drop reduced by the Ohmic potential drop, $\Delta\varphi_{Ohm}$, determined by the resistance of the non-polarized membrane system [68]. $\Delta\varphi_{Ohm}$ value is found by the extrapolation of chronopotentiogram in $\Delta\varphi - t^{0.5}$ coordinates to time t=0 (the moment of switching on the current) [29].

two adjacent diffusion layers of thickness δ are considered. The fluxes are described by the Nernst-Planck equations under the assumption of local electroneutrality. The transition time in this model, like as in the Sand model, is found as the time corresponding to zero interfacial concentration, hence, to infinitely high potential drop (Fig. 5). As Fig. 5 shows, really, τ_{theor} is higher than τ_{Sand}, but remains lower than τ_{exp}. Below we discuss the obtained results.

As Figs. 5 and 6 show, there is a monotonous increase of (reduced) potential drop, Δφ′, with time, t, when t is small, and the experimental chronopotentiograms match well the theoretical one. However, the divergence of curves appears after some threshold time is reached. At time t_m, which is smaller than the transition time, a delay of potential growth occurs in experimental chronopotentiogram, leading (in this case) to formation of a local maximum. However, after a few of seconds, Δφ′ restarts to grow. Similar behavior of chronopotentio-

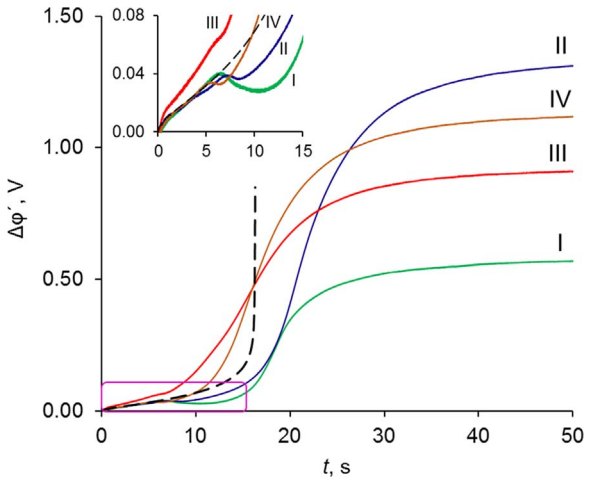

Fig. 6. Initial portions of chronopotentiograms of studied membranes (solid lines) and the chronopotentiogram calculated using the three-layer model (dashed line) obtained for i=4.5 mA cm^{-2}. The samples are denoted as follows: AMX-Sb (I), AMX-Sb$_{used}$ (II), AMX-Sb$_{mod1}$ (III), AMX-Sb$_{mod2}$ (IV).

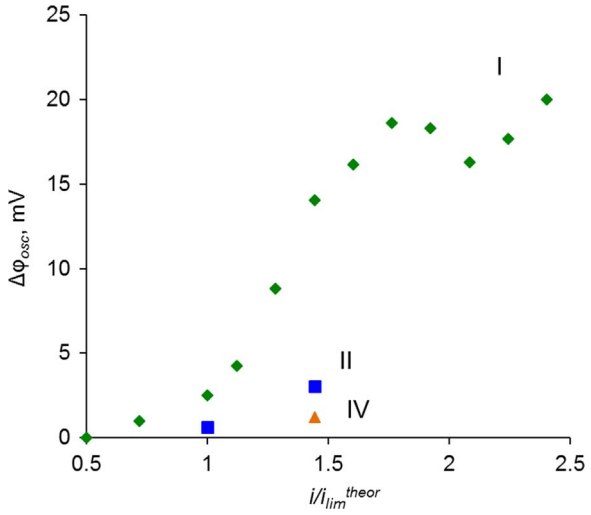

Fig. 7. The depth of potential decrease in the first oscillation, $\Delta\varphi_{osc}$, vs. the ratio of the current density to its limiting value. The data are for AMX-Sb (I), AMX-Sb_{used} (II) and AMX-Sb_{mod2} (IV).

grams of AMX-Sb membrane was observed in [28] and was interpreted as a superposition of the monotonous growth of the potential drop, caused by globally increasing concentration polarization, and an oscillation of potential due to early appearing electroconvection. The difference in Δφ′ between the local maximum and the local minimum is denoted as $\Delta\varphi_{osc}$.

In case of AMX-Sb membrane, the delay of potential growth in chronopotentiogram is observed at i≥2.3 mA cm^{-2} ($i/i_{lim}{}^{theor}$ ≥0.74) (Fig. 6). For all other samples this delay is found starting from 3.0 mA cm^{-2} ($i/i_{lim}{}^{theor}$=0.96). For AMX-Sb, AMX-Sb_{used} and AMX-Sb_{mod2} the delay is sufficiently high and leads to formation of local maximum of Δφ′(t). The difference $\Delta\varphi_{osc}$ between the local maximum of Δφ′ and the following minimum registered for the AMX-Sb is the biggest among the studied samples (Figs. 6, 7). In case of AMX-Sb_{mod1}, the delay is also detectable, but it is too small for the formation of local extremum.

The parameters of oscillations in potential drop on the chronopotentiograms obtained at i=4.5 mA cm^{-2} ($i/i_{lim}{}^{theor}$=1.44) and the results of the contact angle and zeta potential measurements are given in Table 2.

The evaluation of γ made basing on micrographs shown in Figs. 1 and 2, when the relief is approximated with semiellipses, gives 1.2 and 1.1, respectively. For calculation ζ with Eq. (9), we take γ=1.15, the value of κ_m is presented in Table 1and measured value of κ_0 was 0.131 S m^{-1}, h=70 μm, d_m=134 μm, Du=0.

The effective surface charge density found when applying Eq. (2) from the value of ζ calculated using the Helmholtz-Smoluchowski equation, Eq. (4), is essentially lower than the surface charge density evaluated from the exchange capacity, Q, which is about 1.45 meq cm^{-3} [54]. When assuming the distribution of the fixed charges in the nodes of a cubic lattice, we find the distance M between two neighboring charges as $M=(e\cdot Q^{-1}F)^{1/3}\approx 1$ nm, where e is the charge of an electron ($1.6\cdot10^{-9}$ C). Then the surface charge density is $\sigma=e\cdot M^{-2}\approx 14$ μC cm^{-2}. The value of ζ can be evaluated through the Donnan potential drop at the membrane surface: $\Delta\varphi_D=(\frac{RT}{F})\ln\left(\frac{Q}{c_0}\right)\approx 110$ mV. The above evaluations of ζ and σ are essentially higher than the values found using Eqs. (2) and (4) (Table 2). However, the values of ζ and σ found when applying Eqs. (2) and (9) seem too high. This may be explained by the underestimated roughness of surface expressed by parameter γ. Along with the undulations presented in Fig. 3 ("hills" and "valleys" of the scale of several tens of micron), which are taken into account when founding γ=1.15, there is finer relief at micrometer scale seen in Fig. 2. Nevertheless this and even more finer scales of roughness is difficult to evaluate. In this study, important is the relative variation of ζ and σ when passing from one sample to another.

The fact that the initial portion of the chronopotentiograms obtained for the AMX-Sb, AMX-Sb_{used} and AMX-Sb_{mod2} samples matches well the theoretical curve evidences that for these membranes, the concentration profile is formed in a similar way and this process is described by planar diffusion across a finite-length diffusion layer. However, in the case of AMX-Sb_{mod1} membrane the rate of potential increase is higher at the beginning of chronopotentiogram; the value of transition time is the smallest one among the studied cases. This behavior may be explained by the fact that a thin (estimated as a few of μm) layer casted from a MF-4SK solution could cover only partly the AMX-Sb surface: the regions where the layer of MF-4SK is present alternate with the regions where this layer is absent or too thin. Then the surface gets electrically heterogeneous. As it was shown experimentally by Volodina [71] and theoretically by Mareev [72], due to the funneling effect [73] (accumulation of current lines within the well conducting areas of the surface, and the curvature of current lines), the potential drop increases more rapidly and the transition time is lower than in the case of electrically homogeneous membranes.

After initial monotonous growth of Δφ′, there is a delay in the rate of this growth, expressed even by a lowering of Δφ′ for three membranes from four studied. Note that the depth of the first decrease of potential drop ($\Delta\varphi_{osc}$) diminishes with decreasing the absolute value of zeta-potential (Table 2): AMX-Sb > AMX-Sb_{used} > AMX-Sb_{mod2} > AMX-Sb_{mod1}. That allows one to assume that the main cause of potential drop decrease is the classical electroosmosis and the main factor affected EC is the absolute value of the surface charge.

When the transition time is passed, the rate of potential growth decreases for all membranes, in all cases the systems approaches a steady state. The steady-state value of Δφ′ increases in the following order: AMX-Sb < AMX-Sb_{mod1} < AMX-Sb_{mod2} < AMX-Sb_{used}. We can see that the AMX-Sb membrane is always the best one. However, the

Table 2
Electrochemical (obtained at i=4.5 mA cm^{-2} ($i/i_{lim}{}^{theor}$=1.44)) and surface properties of studied membranes.

Sample	IAMX-Sb	IIAMX-Sb_{used}	IIIAMX-Sb_{mod1}	IVAMX-Sb_{mod2}
Contact angle, degrees	63	74	117	85
Streaming potential coefficient, mV bar^{-1}	15.1	4.1	−0.4	−0.8
Zeta potential, mV, Eq.(4)	27.5	7.4	−0.7	−1.5
Surface charge, μC cm^{-2}, Eqs.(4) and (2)	0.95	0.24	−0.02	−0.05
Zeta potential, mV, Eq.(9)	247.5	66.7	−6.1	−13.9
Surface charge, μC cm^{-2}, Eqs.(9) and (2)	111.6	2.9	0.2	0.46
Experimental transition time[a], τ_{exp}, s	18.1	18.5	15.4	15.5
Potential drop at steady state, mV	640	1390	960	1180
Time of the first local maximum of Δφ′, t_m, s	6.4	7.2	6.0	5.5
Value of Δφ′ at the first local maximum, mV	43	39	64	36
Depth of Δφ′ decrease in the first oscillation, $\Delta\varphi_{osc}$, mV	14	3	–	1

[a] The transition time given by the Sand equation, Eq. (11), τ_{Sand} =14.8 s

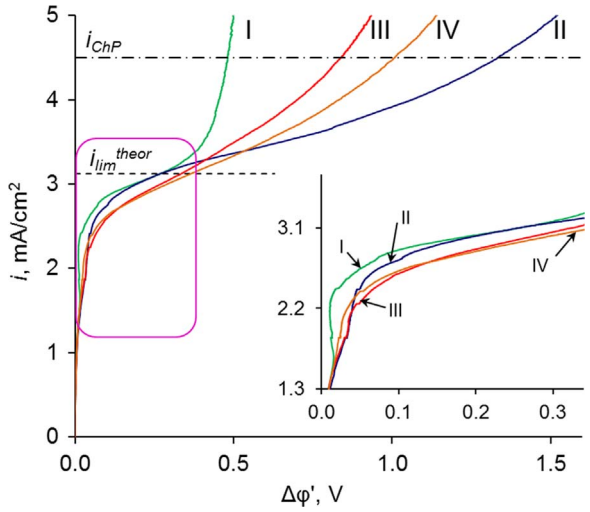

Fig. 8. Current-voltage characteristics (solid lines) of AMX-Sb (I), AMX-Sb_{used} (II), AMX-Sb_{mod1} (III) and AMX-Sb_{mod2} (IV). The dashed line shows the limiting current density calculated by Eq. (3). The dash-dot line shows the current density, at which the chronopotentiograms in Fig. 5 were obtained.

AMX-Sb_{used} membrane, which is the second after the AMX-Sb in the initial portion of the chronopotentiogram, shows the biggest potential drop in the steady state. The AMX-Sb_{mod1} membrane, which is the most hydrophobic and which produces the biggest potential drop in the initial portion, shows the second result after the AMX-Sb in steady state. It makes us think that the main factor determining the intensity of electroconvection in the steady state is the surface hydrophobicity, as it was concluded earlier [33,34].

Similar conclusions follow from the analysis of the current-voltage characteristics (Fig. 8). At small currents, $i \ll i_{lim}^{theor}$, the I-V curves of all membranes are monotonous and the difference between them is negligible. When approaching the limiting current, Δφ′ being in the range 0.03–0.06 V, the deviations from linearity are observed. Note that in the case of AMX-Sb and AMX-Sb_{used}, Δφ′ decreases with increasing current density in the range between 1.7 and 2.5 mA cm^{-2} ($0.54 < i_{lim}^{theor} < 0.80$). This behavior correlates well with that observed in chronopotentiograms, and the range of Δφ′ where a decrease in potential is observed is the same. The value of current density under a given Δφ′ in current-voltage characteristics decreases in the same order in which $\Delta\varphi_{osc}$ decreases in chronopotentiograms: AMX-Sb > AMX-Sb_{used} > AMX-Sb_{mod2} > AMX-Sb_{mod1}. Keep in mind that this order also relates to decreasing the absolute value of the surface charge.

At relatively high values of overlimiting current ($i > 3.5$ mA cm^{-2}, $i/i_{lim}^{theor} > 1.12$) the quasi-steady-state values of potential drop in the I-V curves increase in the same order as the steady-state potential drops found in chronopotentiometric measurements: AMX-Sb < AMX-Sb_{mod1} < AMX-Sb_{mod2} < AMX-Sb_{used}.

As it was found earlier when studying the behavior of other membranes [28], the main mechanism responsible for the earlier oscillations of potential drop is equilibrium EC. It was shown that at the salt concentration and intermembrane distance used in this work, the contribution of gravitational convection [5] to mass transfer is negligible. The absence of another possible mechanism of overlimiting current increase, generation of H^+ and OH^- ions at the depleted membrane/solution interface, is proven by the control of pH difference between the entrance and the exit of desalination channel.

The time when the first oscillation in chronopotentiogram occurs is far smaller than the transition time. Deviations of current-voltage characteristics from monotonous course also appear before the limiting current density is reached. The corresponding potential drops where these “anomalies” occur (about 0.03–0.06 V) are too small for initiating nonequilibrium EC (electroosmosis of the first kind), according to simulations made in [20]. Thus we conclude that the only possible mechanism of potential oscillations in chronopotentiograms and “anomalous” course of current-voltage characteristics is equilibrium EC. This conclusion is supported by the order in which the values of oscillations increase for the studied membrane: it is the order of increasing the absolute value of surface charge/zeta potential.

The changes in the order of the I-V curves and chronopotentiograms occurring after the transition to overlimiting currents are apparently caused by the development of nonequilibrium EC (electroosmosis of the second kind). Here in the range of current densities starting from i_{lim} and up to about 1.2 i_{lim}, the current-voltage characteristics are smooth that relates to the stable EO of the Dukhin-Mishchuk mode. At $i > 1.2\ i_{lim}$, oscillations may be observed suggesting that the EC mode transfers to the Rubinstein-Zaltzman one. As previously mentioned, the development of nonequilibrium EC is mainly determined by the size of extended SCR, which becomes several orders of magnitude bigger than the thickness of equilibrium EDL. Hence the value of the surface space charge, which determines the charge in the equilibrium EDL, plays in this case a secondary role. The effect of surface hydrophobicity becomes more important [28,33], since higher hydrophobicity reduces the impediment in the development of vortices produced by water cling to the surface. This is the reason why in the order describing EC intensity at high currents, the AMX-Sb_{mod1} and AMX-Sb_{mod2} samples stand before the AMX-Sb_{used}: the AMX-Sb_{mod1} membrane, which possesses the highest surface hydrophobicity among the all studied samples, generates a more intensive nonequilibrium EC compared to the AMX-Sb_{used} and AMX-Sb_{mod2}. When comparing the properties of AMX-Sb and all other samples, we may assume that the significantly higher surface charge of this membrane remains the decisive factor, which allows generation more intensive EC at high currents despite its lesser hydrophobicity. Another factor, which may affect EC, is the surface undulation, which is lower after casting MF-4SK on the AMX-Sb surface.

4. Conclusion

We have studied, for the first time, the impact of ion-exchange membrane surface charge on the intensity and the mode of EC. Four samples of anion-exchange membranes with the same surface geometry and differing in the surface charge and the degree of hydrophobicity were studied. It is found that the changes in the surface charge, evaluated through the zeta-potential, and in the degree of surface hydrophobicity, evaluated by the contact angle, affect the shape of chronopotentiograms and current-voltage characteristics. The value of the surface charge has the crucial importance for the development of oscillations in the chronopotentiograms occurring at $i > i_{lim}$ and low voltages before the transition time is reached. It also affects the shape of the current-voltage characteristics in the range between 1.7 and 2.5 mA cm^{-2} ($0.54 < i/i_{lim} < 0.80$). In this range, for the membranes with a high surface charge, an anomaly occurs: with increasing current density the steady-state potential drop is decreasing instead of increasing. The corresponding potential drops in all cases, where the impact of surface charge is dominant, lay in the range of 0.03–0.06 V, which suggests that the reason for the changes of chronopotentiograms and current-voltage characteristics is the equilibrium EC developed by the mechanism of electroosmosis of the first kind. In this mode, the (quasi)equilibrium EDL, whose parameters are determined by the surface charge, plays the main role in the development of EC. High surface charge implies a hydrophilic surface.

The surface hydrophobicity has more influence on the chronopotentiograms and current-voltage characteristics, when the potential drop is higher than approximately 0.4 V that corresponds to the voltage at which the limiting current density is reached in (quasi)steady state. Then the extended SCR is formed and EC becomes nonequilibrium occurring apparently as electroosmosis of the second kind. In this mode, the (quasi)equilibrium EDL is less important; EC is governed by

the extended SCR. Higher hydrophobicity reduces the impediment in the development of vortices produced by water cling to the surface.

Acknowledgements

This research was financially supported by the Russian Foundation of Basic Research, Grant no. 15-58-16005 (experimental study of electroconvection at low potential drops), and by the Russian Science Foundation, Grant no. 14-19-00401 (preparation of the membranes and the study of the effect of surface charge on electroconvection).

References

[1] H. Strathmann, Electrodialysis, a mature technology with a multitude of new applications, Desalination 264 (2010) 268–288. http://dx.doi.org/10.1016/j.desal.2010.04.069.
[2] P. Długołęcki, B. Anet, S.J. Metz, K. Nijmeijer, M. Wessling, Transport limitations in ion exchange membranes at low salt concentrations, J. Membr. Sci. 346 (2010) 163–171. http://dx.doi.org/10.1016/j.memsci.2009.09.033.
[3] P. Długołęcki, P. Ogonowski, S.J. Metz, M. Saakes, K. Nijmeijer, M. Wessling, On the resistances of membrane, diffusion boundary layer and double layer in ion exchange membrane transport, J. Membr. Sci. 349 (2010) 369–379. http://dx.doi.org/10.1016/j.memsci.2009.11.069.
[4] I. Rubinstein, L. Shtilman, Voltage against current curves of cation exchange membranes, J. Chem. Soc. Faraday Trans. 2 75 (1979) 231–246. http://dx.doi.org/10.1039/f29797500231.
[5] V.I. Zabolotsky, V.V. Nikonenko, N.D. Pismenskaya, E.V. Laktionov, M.K. Urtenov, H. Strathmann, et al., Coupled transport phenomena in overlimiting current electrodialysis, Sep. Purif. Technol. 14 (1998) 255–267. http://dx.doi.org/10.1016/S1383-5866(98)00080-X.
[6] R. Simons, Strong electric field effects on proton transfer between membrane-bound amines and water, Nature 280 (1979) 824–826. http://dx.doi.org/10.1038/280824a0.
[7] V.I. Zabolotskii, N.V. Shel'deshov, N.P. Gnusin, Dissociation of water molecules in systems with ion-exchange membranes, Russ. Chem. Rev. 57 (1988) 801–808. http://dx.doi.org/10.1070/RC1988v057n08ABEH003389.
[8] S.J. Kim, Y.-C. Wang, J.H. Lee, H. Jang, J. Han, Concentration polarization and nonlinear electrokinetic flow near a nanofluidic channel, Phys. Rev. Lett. 99 (2007) 44501. http://dx.doi.org/10.1103/PhysRevLett.99.044501.
[9] J. de Jong, R.G.H. Lammertink, M. Wessling, Membranes and microfluidics: a review, Lab Chip 6 (2006) 1125–1139. http://dx.doi.org/10.1039/b603275c.
[10] D.-T. Phan, S.A.M. Shaegh, C. Yang, N.-T. Nguyen, Sample concentration in a microfluidic paper-based analytical device using ion concentration polarization, Sens. Actuators B Chem. 222 (2016) 735–740. http://dx.doi.org/10.1016/j.snb.2015.08.127.
[11] M. Rosso, Electrodeposition from a binary electrolyte: new developments and applications, Electrochim. Acta 53 (2007) 250–256. http://dx.doi.org/10.1016/j.electacta.2007.02.026.
[12] M.A.K. Urtenov, E.V. Kirillova, N.M. Seidova, V.V. Nikonenko, Decoupling of the Nernst-Planck and Poisson equations. Application to a membrane system at overlimiting currents, J. Phys. Chem. B 111 (2007) 14208–14222. http://dx.doi.org/10.1021/jp073103d.
[13] I. Rubinstein, B. Zaltzman, Equilibrium electroconvective instability, Phys. Rev. Lett. 114 (2015) 1–5. http://dx.doi.org/10.1103/PhysRevLett.114.114502.
[14] S.S. Dukhin, Electrokinetic phenomena of the second kind and their applications, Adv. Colloid Interface Sci. 35 (1991) 173–196. http://dx.doi.org/10.1016/0001–8686(91)80022-C.
[15] S.S. Dukhin, N.A. Mishchuk, P.V. Takhistov, Electroosmosis of the second kind and unrestricted current increase in the mixed monolayer of an ion-exchanger, Colloied J. USSR 51 (1989) 540–542.
[16] N.A. Mishchuk, Electro-osmosis of the second kind near the heterogeneous ion-exchange membrane, Colloids Surf. A Physicochem. Eng. Asp. 140 (1998) 75–89. http://dx.doi.org/10.1016/S0927-7757(98)00216-7.
[17] N.A. Mishchuk, P.V. Takhistov, Electroosmosis of the second kind, Colloids Surf. A Physicochem. Eng. Asp. 95 (1995) 119–131. http://dx.doi.org/10.1016/0927–7757(94)02988-5.
[18] I. Rubinstein, B. Zaltzman, Electro-osmotically induced convection at a permselective membrane, Phys. Rev. E Stat. Phys. Plasmas Fluids Relat. Interdiscip. Top. 62 (2000) 2238–2251. http://dx.doi.org/10.1103/PhysRevE.62.2238.
[19] V.S. Pham, Z. Li, K.M. Lim, J.K. White, J. Han, Direct numerical simulation of electroconvective instability and hysteretic current-voltage response of a permselective membrane, Phys. Rev. E - Stat. Nonlinear Soft Matter Phys. 86 (2012) 1–11. http://dx.doi.org/10.1103/PhysRevE.86.046310.
[20] M.K. Urtenov, A.M. Uzdenova, A.V. Kovalenko, V.V. Nikonenko, N.D. Pismenskaya, V.I. Vasil'eva, et al., Basic mathematical model of overlimiting transfer enhanced by electroconvection in flow-through electrodialysis membrane cells, J. Membr. Sci. 447 (2013) 190–202. http://dx.doi.org/10.1016/j.memsci.2013.07.033.
[21] E.A. Demekhin, N.V. Nikitin, V.S. Shelistov, Direct numerical simulation of electrokinetic instability and transition to chaotic motion, Phys. Fluids 25 (2013) 122001. http://dx.doi.org/10.1063/1.4843095.
[22] S.M. Davidson, M. Wessling, A. Mani, On the dynamical regimes of pattern-accelerated electroconvection, Sci. Rep. 6 (2016) 22505. http://dx.doi.org/10.1038/srep22505.
[23] E.I. Belova, G.Y. Lopatkova, N.D. Pismenskaya, V.V. Nikonenko, C. Larchet, G. Pourcelly, Effect of anion-exchange membrane surface properties on mechanisms of overlimiting mass transfer, J. Phys. Chem. B 110 (2006) 13458–13469. http://dx.doi.org/10.1021/jp062433f.
[24] M. Wessling, L.G. Morcillo, S. Abdu, Nanometer-thick lateral polyelectrolyte micropatterns induce macrosopic electro-osmotic chaotic fluid instabilities, Sci. Rep. 4 (2014) 4294. http://dx.doi.org/10.1038/srep04294.
[25] J.C. de Valença, R.M. Wagterveld, R.G.H. Lammertink, P.A. Tsai, Dynamics of microvortices induced by ion concentration polarization, Phys. Rev. E 92 (2015) 31003. http://dx.doi.org/10.1103/PhysRevE.92.031003.
[26] B. Zaltzman, I. Rubinstein, Electro-osmotic slip and electroconvective instability, J. Fluid Mech. 579 (2007) 173–226. http://dx.doi.org/10.1017/S0022112007004880.
[27] E.K. Zholkovskij, M.A. Vorotyntsev, E. Staude, Electrokinetic instability of solution in a plane-parallel electrochemical cell, J. Colloid Interface Sci. 181 (1996) 28–33. http://dx.doi.org/10.1006/jcis.1996.0353.
[28] E. Korzhova, N. Pismenskaya, D. Lopatin, O. Baranov, L. Dammak, V. Nikonenko, Effect of surface hydrophobization on chronopotentiometric behavior of an AMX anion-exchange membrane at overlimiting currents, J. Membr. Sci. 500 (2016) 161–170. http://dx.doi.org/10.1016/j.memsci.2015.11.018.
[29] V.V. Gil, M.A. Andreeva, N.D. Pismenskaya, V.V. Nikonenko, C. Larchet, L. Dammak, Effect of counterion hydration number on the development of electroconvection near the surface of heterogeneous cation-exchange membrane modified by a MF-4SK film, Pet. Chem. 6 (2016).
[30] H.-J. Butt, K. (Karlheinz) Graf, M. Kappl, Physics and Chemistry of Interfaces, Wiley-VCH, Germany, 2006.
[31] M.B. Andersen, M. Van Soestbergen, A. Mani, H. Bruus, P.M. Biesheuvel, M.Z. Bazant, Current-induced membrane discharge, Phys. Rev. Lett. 109 (2012), 108301. http://dx.doi.org/10.1103/PhysRevLett.109.108301.
[32] A.D. Stroock, M. Weck, D.T. Chiu, W.T.S. Huck, P.J.A. Kenis, R.F. Ismagilov, et al., Patterning electro-osmotic flow with patterned surface charge, Phys. Rev. Lett. 84 (2000) 3314–3317. http://dx.doi.org/10.1103/PhysRevLett.84.3314.
[33] E.D. Belashova, N.A. Melnik, N.D. Pismenskaya, K.A. Shevtsova, A.V. Nebavsky, K.A. Lebedev, et al., Overlimiting mass transfer through cation-exchange membranes modified by Nafion film and carbon nanotubes, Electrochim. Acta 59 (2012) 412–423. http://dx.doi.org/10.1016/j.electacta.2011.10.077.
[34] N.D. Pismenskaya, V.V. Nikonenko, N.A. Melnik, K.A. Shevtsova, E.I. Belova, G. Pourcelly, et al., Evolution with time of hydrophobicity and microrelief of a cation-exchange membrane surface and its impact on overlimiting mass transfer, J. Phys. Chem. B 116 (2012) 2145–2161. http://dx.doi.org/10.1021/jp2101896.
[35] V.S. Shelistov, E.A. Demekhin, G.S. Ganchenko, Electrokinetic instability near charge-selective hydrophobic surfaces, Phys. Rev. E - Stat. Nonlinear Soft Matter Phys. 90 (2014), 013001. http://dx.doi.org/10.1103/PhysRevE.90.013001.
[36] M. Bazant, O. Vinogradova, Tensorial hydrodynamic slip, J. Fluid Mech. 613 (2008) 125–134. http://dx.doi.org/10.1017/S002211200800356X.
[37] N. Mishchuk, Electric double layer and electrostatic interaction of hydrophobic particles, J. Colloid Interface Sci. 320 (2008) 599–607. http://dx.doi.org/10.1016/j.jcis.2007.12.047.
[38] D.A. Doshi, E.B. Watkins, J.N. Israelachvili, J. Majewski, Reduced water density at hydrophobic surfaces: effect of dissolved gases, Proc. Natl. Acad. Sci. U.S.A. 102 (2005) 9458–9462. http://dx.doi.org/10.1073/pnas.0504034102.
[39] M. Mezger, H. Reichert, S. Schöder, J. Okasinski, H. Schröder, H. Dosch, et al., High-resolution in situ x-ray study of the hydrophobic gap at the water-octadecyltrichlorosilane interface, Proc. Natl. Acad. Sci. U.S.A. 103 (2006) 18401–18404. http://dx.doi.org/10.1073/pnas.0608827103.
[40] N.V. Churaev, V.D. Sobolev, A.N. Somov, Slippage of liquids over lyophobic solid surfaces, J. Colloid Interface Sci. 97 (1984) 574–581. http://dx.doi.org/10.1016/0021–9797(84)90330-8.
[41] S.R. Maduar, A.V. Belyaev, V. Lobaskin, O.I. Vinogradova, Electrohydrodynamics near hydrophobic surfaces, Phys. Rev. Lett. 114 (2015) 1–5. http://dx.doi.org/10.1103/PhysRevLett.114.118301.
[42] N.A. Mishchuk, The model of hydrophobic attraction in the framework of classical DLVO forces, Adv. Colloid Interface Sci. 168 (2011) 149–166. http://dx.doi.org/10.1016/j.cis.2011.06.003.
[43] C.I. Bouzigues, P. Tabeling, L. Bocquet, Nanofluidics in the debye layer at hydrophilic and hydrophobic surfaces, Phys. Rev. Lett. 101 (2008) 114503. http://dx.doi.org/10.1103/PhysRevLett.101.114503.
[44] A. Yaroshchuk, T. Luxbacher, Interpretation of electrokinetic measurements with porous films: role of electric conductance and streaming current within porous structure, Langmuir 26 (2010) 10882–10889. http://dx.doi.org/10.1021/la100777z.
[45] P. Fievet, M. Sbaï, A. Szymczyk, A. Vidonne, Determining the ζ-potential of plane membranes from tangential streaming potential measurements: effect of the membrane body conductance, J. Membr. Sci. 226 (2003) 227–236. http://dx.doi.org/10.1016/j.memsci.2003.09.007.
[46] A. Szymczyk, N. Fatin-Rouge, P. Fievet, Tangential streaming potential as a tool in modeling of ion transport through nanoporous membranes, J. Colloid Interface Sci. 309 (2007) 245–252. http://dx.doi.org/10.1016/j.jcis.2007.02.005.
[47] A. Szymczyk, Y.I. Dirir, M. Picot, I. Nicolas, F. Barrière, Advanced electrokinetic characterization of composite porous membranes, J. Membr. Sci. 429 (2013) 44–51. http://dx.doi.org/10.1016/j.memsci.2012.11.076.
[48] M.D. Afonso, G. Hagmeyer, R. Gimbel, Streaming potential measurements to assess the variation of nanofiltration membranes surface charge with the concentration of salt solutions, Sep. Purif. Technol. 22–23 (2001) 529–541. http://dx.doi.org/10.1016/S1383-5866(00)00135-0.

[49] J.-S. Park, H.-J. Lee, S.-J. Choi, K.E. Geckeler, J. Cho, S.-H. Moon, Fouling mitigation of anion exchange membrane by zeta potential control, J. Colloid Interface Sci. 259 (2003) 293–300. http://dx.doi.org/10.1016/S0021-9797(02)00095-4.
[50] Y. Sedkaoui, A. Szymczyk, H. Lounici, O. Arous, A new lateral method for characterizing the electrical conductivity of ion-exchange membranes, J. Membr. Sci. 507 (2016) 34–42. http://dx.doi.org/10.1016/j.memsci.2016.02.003.
[51] H.-J. Lee, J.-H. Choi, J. Cho, S.-H. Moon, Characterization of anion exchange membranes fouled with humate during electrodialysis, J. Membr. Sci. 203 (2002) 115–126. http://dx.doi.org/10.1016/S0376-7388(01)00792-X.
[52] E. Güler, W. van Baak, M. Saakes, K. Nijmeijer, Monovalent-ion-selective membranes for reverse electrodialysis, J. Membr. Sci. 455 (2014) 254–270. http://dx.doi.org/10.1016/j.memsci.2013.12.054.
[53] Astom corporation ion exchange membranes, (n.d.). ⟨http://www.astom-corp.jp/en/product/10.html⟩.
[54] X.T. Le, Permselectivity and microstructure of anion exchange membranes, J. Colloid Interface Sci. 325 (2008) 215–222. http://dx.doi.org/10.1016/j.jcis.2008.05.050.
[55] J.H. Choi, S.-H. Moon, Structural change of ion-exchange membrane surfaces under high electric fields and its effects on membrane properties, J. Colloid Interface Sci. 265 (2003) 93–100. http://dx.doi.org/10.1016/S0021-9797(03)00136-X.
[56] V.I. Zabolotskii, R.K. Chermit, M.V. Sharafan, Mass transfer mechanism and chemical stability of strongly basic anion-exchange membranes under overlimiting current conditions, Russ. J. Electrochem. 50 (2014) 38–45. http://dx.doi.org/10.1134/S102319351401011X.
[57] V.I. Vasil'Eva, A.V. Zhil'Tsova, M.D. Malykhin, V.I. Zabolotskii, K.A. Lebedev, R.K. Chermit, et al., Effect of the chemical nature of the ionogenic groups of ion-exchange membranes on the size of the electroconvective instability region in high-current modes, Russ. J. Electrochem. 50 (2014) 134–143. http://dx.doi.org/10.1134/S1023193514020062.
[58] G. Merle, M. Wessling, K. Nijmeijer, Anion exchange membranes for alkaline fuel cells: a review, J. Membr. Sci. 377 (2011) 1–35. http://dx.doi.org/10.1016/j.memsci.2011.04.043.
[59] L. Franck-Lacaze, P. Sistat, P. Huguet, Determination of the pKa of poly (4-vinylpyridine)-based weak anion exchange membranes for the investigation of the side proton leakage, J. Membr. Sci. 326 (2009) 650–658. http://dx.doi.org/10.1016/j.memsci.2008.10.054.
[60] K.G. Sabbatovskii, A.I. Vilenskii, V.D. Sobolev, Electrosurface properties of poly(-ethylene terephthalate) films irradiated by heavy ions and track membranes based on these films, Colloid J. 78 (2016) 573–575. http://dx.doi.org/10.1134/S1061933×1604013X.
[61] J. Newman, K.E. Thomas-Alyea, Electrochem. Syst. (2004). http://dx.doi.org/10.1086/421629.
[62] G. Hagmeyer, R. Gimbel, Modelling the salt rejection of nanofiltration membranes for ternary ion mixturs and for single salts at different pH values, Desalination 117 (1998) 247–256. http://dx.doi.org/10.1016/S0011-9164(98)00109-X.
[63] J. Lukáš, K. Richau, H.H. Schwarz, D. Paul, Surface characterization of polyelectrolyte complex membranes based on sodium cellulose sulfate and various cationic components, J. Membr. Sci. 131 (1997) 39–47. http://dx.doi.org/10.1016/S0376-7388(97)00009-4.
[64] A. Yaroshchuk, V. Ribitsch, Role of channel wall conductance in the determination of ζ-potential from electrokinetic measurements, Langmuir 18 (2002) 2036–2038. http://dx.doi.org/10.1021/la015557m.
[65] A.V. Delgado, F. González-Caballero, R.J. Hunter, L.K. Koopal, J. Lyklema, Measurement and interpretation of electrokinetic phenomena, J. Colloid Interface Sci. 309 (2007) 194–224. http://dx.doi.org/10.1016/j.jcis.2006.12.075.
[66] R.J. Hunter, Zeta Potential in Colloid Science: Principles and Applications, Academic Press, San Diego, 1981.
[67] C. Larchet, S. Nouri, B. Auclair, L. Dammak, V. Nikonenko, Application of chronopotentiometry to determine the thickness of diffusion layer adjacent to an ion-exchange membrane under natural convection, Adv. Colloid Interface Sci. 139 (2008) 45–61. http://dx.doi.org/10.1016/j.cis.2008.01.007.
[68] H.W. Rösler, F. Maletzki, E. Staude, Ion transfer across electrodialysis membranes in the overlimiting current range: chronopotentiometric studies, J. Membr. Sci. 72 (1992) 171–179. http://dx.doi.org/10.1016/0376–7388(92)80197-R.
[69] S.A. Mareev, D.Y. Butylskii, N.D. Pismenskaya, V.V. Nikonenko, Chronopotentiometry of ion-exchange membranes in the overlimiting current range. Transition time for a finite-length diffusion layer: modeling and experiment, J. Membr. Sci. 500 (2016) 171–179. http://dx.doi.org/10.1016/j.memsci.2015.11.026.
[70] M. Van Soestbergen, P.M. Biesheuvel, M.Z. Bazant, Diffuse-charge effects on the transient response of electrochemical cells, Phys. Rev. E - Stat. Nonlinear Soft Matter Phys. 81 (2010) 1–13. http://dx.doi.org/10.1103/PhysRevE.81.021503.
[71] E. Volodina, N. Pismenskaya, V. Nikonenko, C. Larchet, G. Pourcelly, Ion transfer across ion-exchange membranes with homogeneous and heterogeneous surfaces, J. Colloid Interface Sci. 285 (2005) 247–258. http://dx.doi.org/10.1016/j.jcis.2004.11.017.
[72] S.A. Mareev, V.S. Nichka, D.Y. Butylskii, M.K. Urtenov, N.D. Pismenskaya, P.Y. Apel, et al., Chronopotentiometric response of an electrically heterogeneous permselective surface: 3d modeling of transition time and experiment, J. Phys. Chem. C 120 (24) (2016) 13113–13119. http://dx.doi.org/10.1021/acs.jpcc.6b03629.
[73] I. Rubinstein, B. Zaltzman, T. Pundik, Ion-exchange funneling in thin-film coating modification of heterogeneous electrodialysis membranes, Phys. Rev. E - Stat. Nonlinear Soft Matter Phys. 65 (2002) 1–10. http://dx.doi.org/10.1103/PhysRevE.65.041507.